

# Abelian Manna model on various lattices in one and two dimensions

Hoai Nguyen Huynh,<sup>1,\*</sup> Gunnar Pruessner,<sup>2,†</sup> and Lock Yue Chew<sup>1,‡</sup>

<sup>1</sup>*Division of Physics and Applied Physics, School of Physical and Mathematical Sciences,  
Nanyang Technological University, Singapore, 21 Nanyang Link, Singapore 637371*

<sup>2</sup>*Department of Mathematics, Imperial College London,  
180 Queen's Gate, London SW7 2BZ, United Kingdom*

(Dated: September 24, 2018)

We perform a high-accuracy moment analysis of the avalanche size, duration and area distribution of the Abelian Manna model on eight two-dimensional and four one-dimensional lattices. The results provide strong support to establish universality of exponents and moment ratios across different lattices and a good survey for the strength of corrections to scaling which are notorious in the Manna universality class. The results are compared against previous work done on Manna model, Oslo model and directed percolation. We also confirm hypothesis of various scaling relations.

PACS numbers: 05.65.+b, 05.70.Jk

Keywords: Self-organized criticality, Lattices, Universality, Finite-size scaling, Scaling relations, Moments

## 1. INTRODUCTION

Universality is the key feature of critical systems which justifies the analysis of (over-) simplified numerical models of otherwise much more complex natural systems. When the concept of self-organised criticality (SOC) was introduced [1], it gained immediate popularity on the one hand because it attempted to explain the prevalence of scaling and fractality in nature and on the other hand suggested that many features of very different phenomena would be common to all of them, by the power of universality. At times disputed [2], it is now widely accepted that the predictive power of SOC lies with its universality; the elusive qualities of a critical point, normally confined to a very narrow range of a control parameter, are the norm in SOC models and shared between them.

While universality has been at the centre of the debate about SOC [*e.g.* 3, 4], it comes as a great surprise that it has focused mainly on its occurrence across different models [*e.g.* 5], whereas very little work has been done on establishing it within the same models but across different lattices [*e.g.* 6–9]. Recently, it has been shown [10] that on fractal lattices of same dimension but different structure, the Manna Model [11] behaves very differently. The observation that critical phenomena and scaling displays universal features on different lattices has traditionally been one of the most important insights, enabling, in particular, exact results [12, 13].

During the last decade or so, it has become increasingly clear that SOC is far more elusive than originally envisaged. It is therefore all the more important to establish which features known from ordinary critical phenomena

carry over to SOC. Independence of certain observables from the underlying lattice is one such aspect to substantiate. If universality was not to be found for the same model on different lattices, then the notion of universality in SOC as a whole had to be revised.

In the following, the universality hypothesis in SOC is put to test by simulating the Abelian Manna model (AMM) [11, 14] on different one- and two-dimensional lattices. Owing to their robust scaling behaviour, in recent years, attention has focused on the AMM and the Oslo Model [15], which seem to be in the same universality class [3]. This is contrasted by the poor scaling behaviour of many other established SOC models, such as the Forest Fire Model [16, 17], the Bak-Tang-Wiesenfeld sandpile model [1, 18] or the Olami-Feder-Christensen Model [2, 19].

Apart from probing universality, corrections to scaling can also be tested, with the ultimate aim of finding a lattice that is particularly suited for simulating the AMM. In addition, rarely studied moment ratios are also reported which provide further support for the universality of the AMM. This is of particular interest in one-dimension, where (logarithmic) corrections, are known to be remarkably strong [20].

The following is divided into four parts: In the next section, the model is defined and a few implementation details are discussed, including the method employed to determine the statistical error. All numerical results are collected in Sec. 3 and discussed in Sec. 4.

## 2. MODEL DEFINITION AND METHODS

### 2.1. The Abelian Manna model on an arbitrary lattice

The Abelian Manna model [11, 14, 21] is defined on a lattice  $\mathcal{L}$  with  $N$  sites. Each site  $i$  on  $\mathcal{L}$  has  $q_i$  neighbours, and is assigned to it a non-negative integer variable  $z_i$  which can be thought of as the number of particles at

---

\*Electronic address: hu0004en@e.ntu.edu.sg; URL: <http://www3.ntu.edu.sg/home2008/hu0004en/>

†Electronic address: g.pruessner@imperial.ac.uk; URL: <http://www.ma.ic.ac.uk/~pruess>

‡Electronic address: lockyue@ntu.edu.sg; URL: <http://www.ntu.edu.sg/home/lockyue/>

that site or the height of a stack of particles there. The threshold height at all sites is 1 above which a site is said to be active or unstable, otherwise it is stable. The system evolves as follows. *Driving*: When the system is in a stable or “quiescent” configuration, *i.e.*  $z_i \leq 1$  for all sites, the system is charged by picking a site  $i$  at random and incrementing  $z_i$  by 1. *Relaxation*: Every unstable site  $i$  relaxes by transferring two particles to its neighbours, possibly rendering the receiving site unstable. The recipient of each of the two particles is chosen randomly and independently. Unstable sites are updated in a random sequential order. By virtue of its Abelian nature the order of relaxations is irrelevant for (the statistics of) the final state of the lattice and the statistics of the avalanche size (see below).

Each relaxation of a site constitutes a toppling, which in the bulk is conservative, *i.e.* the total  $\sum_i z_i$  remains unchanged by bulk topplings. A (small) number of sites are considered dissipative boundary sites, which have “virtual” neighbours, that are included in the total count of neighbours  $q_i$  introduced above (but not in the number of sites  $N$ ). Virtual neighbours (or sites) never topple themselves, *i.e.* particles are lost from the system at receipt. Such sites therefore provide a dissipation mechanism, and are introduced here solely as a bookkeeping device. As a general principle, the number of virtual neighbours of sites in the lattices discussed below are always chosen so that the resulting  $q_i$  at a boundary site matches that of a corresponding site in the bulk. In the lattices below,  $q_i$  might take on at most two different values, yet bulk sites and boundary sites do not differ in that respect.

An avalanche is the totality of all topplings until the system is quiescent again. The size  $s$  of the avalanche is measured as the number topplings performed between driving and quiescence, so that  $s = 0$  if no avalanche occurs after the driving. The area  $a$  of an avalanche is the number of distinct sites which received a particle during the avalanche. This includes the site charged by the driving, so that  $a \geq 1$ . The definition of time used to determine the duration  $t$  of an avalanche is based on the idea that each active site undergoes a Poissonian decay, *i.e.* all active sites topple with the same rate. This rate is chosen to be unity, so that on average time  $1/N_a$  goes by until a site topples if  $N_a$  sites are active. This is the amount by which time advances each time a site topples. Each time a site is picked at random, exactly two of its particles are redistributed. This procedure is, of course, not a faithful representation of a true Poisson process, which has random waiting times, but it is an increasingly good approximation in the limit of large activity  $N_a$  [22]. Thanks to its Abelian nature [14], the model’s evolution from quiescent state to quiescent state does not require a specific dynamics on the microscopic time scale, so the definition of time in the present case is to the same degree arbitrary as the dynamics in, say, model A [23].

The Abelian symmetry does not exist in the original model [11], but simplifies its implementation greatly.

Originally, *all* particles were re-distributed at toppling which were subject to parallel updates, so that all sites that were active at time  $t$  had toppled before sites activated by a toppling during that time step. In that version of the model, it takes one time unit to update  $N_a$  simultaneously active sites. In the Abelian version, this holds only for constant  $N_a$  (number of active sites remaining unchanged). Yet, the update rate for both versions is  $1/N_a$  when averaged over suitable intervals (one time unit in the former, one update in the later), although neither is Poissonian. Despite these differences in the definition, Dickman and Campelo [20] have shown that implementing parallel or sequential updating has no noticeable impact on the statistics. They also found that exponents derived from the Abelian variant of the Manna Model coincides with those published for the original version.

## 2.2. The lattices

In the following, we describe four one-dimensional (Fig. 1) and eight two-dimensional lattices (Figs. 2 and 3). In the figures, links to adjacent sites are indicated by solid lines, those to virtual neighbours by dashed ones. As virtual neighbours are merely an accounting device, the positioning of the dashed lines in the figures is arbitrarily chosen to match that of bulk links.

The figures show in particular the boundaries, whose structure we maintained during finite size scaling, *i.e.* when we increased the lattice size, we made sure that the edges and corners of the larger lattice matched that of the smaller one. Initially we dismissed such issues as small corrections, but given the high accuracy with which we determine moments, changes in the boundaries became clearly visible, in particular in the Mitsubishi lattice (Fig. 3(d)). In hindsight this is hardly surprising given the great importance of transport of particles from the conservative bulk to the dissipative boundaries [24].

For some simple lattices, the number of sites  $N$  is exactly the power  $d$  (dimension) of their linear (Euclidean) extension  $L$ . In more complicated cases, this may hold only approximately. In order to maintain a reasonably high symmetry of the finite lattices, which have to be thought of as being cut out of an (infinite) tiling of the plane, we had to make compromises. In one dimension ( $d = 1$ , see Table I),  $N$  is a multiple of  $L$  for the first three lattices discussed. The fourth, the Futatsubishi lattice (Fig. 1(d)), follows  $N = 3L + 1$  for all sizes considered. In two dimensions,  $d = 2$ , two different lengths  $L_x$  and  $L_y$  are introduced for the two different dimensions, defined in a way as natural as possible. The cutting of the finite two-dimensional lattices and the resulting shape of the boundaries was guided by the following principles, which clash and therefore hold only approximately: the number of sites in the lattice  $N = L_x L_y$  had to be as close as possible to the power of 2, the number of sites in a simple square lattice. The ratio  $L_x/L_y$  was to be held

TABLE I: Parameters for the one-dimensional lattices. Only the seven sizes eventually used are listed. The (nominal) linear size  $L$ , corresponding to the examples given in Fig. 1, is shown in brackets.

lattice	$d$	$N$							CPU time (h)
Simple chain	1	1024(1024)	2048(2048)	4096(4096)	8192(8192)	16384(16384)	32768(32768)	65536(65536)	51350
Rope ladder	1	2048(1024)	4096(2048)	8192(4096)	16384(8192)	32768(16384)	65536(32768)	131072(65536)	54299
nnn chain	1	2048(1024)	4096(2048)	8192(4096)	16384(8192)	32768(16384)	65536(32768)	131072(65536)	7943
Futatsubishi	1	3073(1024)	6145(2048)	12289(4096)	24577(8192)	49153(16384)	98305(32768)	196609(65536)	54821

TABLE II: Parameters for the two-dimensional lattices. Only the seven sizes eventually used are listed. The number of sites  $N$  equals the product  $L_x L_y$ .

lattice	$d$	$c_x$	$m_x$	$c_y$	$m_y$	$L_x \times L_y$						CPU time (h)	
Square	2	0	1	0	1	256×256	362×362	512×512	724×724	1024×1024	1448×1448	2048×2048	9530
Jagged	2	1	2	0	1	361×182	511×257	723×363	1023×513	1447×725	2047×1025	2895×1449	9408
Archimedes	2	0	4	0	2	360×182	512×256	724×362	1024×512	1448×724	2048×1024	2896×1448	11106
nc diagonal square	2	1	2	1	2	255×257	361×363	511×513	723×725	1023×1025	1447×1449	2047×2049	9802
Triangular	2	0	1	0	1	239×274	337×389	476×551	673×779	953×1100	1347×1557	1906×2201	6305
Kagomé	2	1	3	0	1	412×159	583×225	826×317	1168×449	1651×635	2335×898	3301×1271	10881
Honeycomb	2	1	2	0	2	337×194	475×276	675×388	953×550	1347×778	1903×1102	2695×1556	7842
Mitsubishi	2	2	3	1	2	239×275	338×387	476×551	674×777	953×1101	1349×1555	1904×2203	7573

constant with increasing  $N$ . The (Euclidean) aspect ratio should be unity or very close, if that clashes with the shape of the boundaries. For each lattice  $m_{x,y}$  and  $c_{x,y}$  were set such that  $L_{x,y} \equiv c_{x,y} \pmod{m_{x,y}}$ , to maintain the shape of the boundaries across different sizes. The parameters and resulting lattice sizes are listed in Table II. The number  $L_y$  can normally be thought as a number of “layers” and  $L_x$  as the number of sites in a layer. It is clear that such a definition, necessary because of the mismatch of the symmetry of lattice to the square symmetry of the cut-out, makes the linear sizes  $L_x$  and  $L_y$  rather poor fitting parameters (see below).

The size of each lattice is indicated exemplarily in the caption of its figure. The sizes of all lattices used in this article are listed in Tables I and II. In the following we describe the lattices in detail.

### 2.2.1. One-dimensional lattices

Simple chain (Fig. 1(a)): This lattice is the usual one-dimensional chain, where each site connects to two nearest neighbours. The leftmost and the rightmost sites have one virtual neighbour each.

Rope ladder (Fig. 1(b)): The shape of this lattice is that of a rope ladder. It is a simple extension of the simple chain (Fig. 1(a)), which eventually leads to the square lattice (Fig. 2(a)). Each site has three nearest neighbours, one on the left, one on the right and one below or above it. Four boundary sites have one virtual neighbour each.

Next nearest neighbour (nnn) chain (Fig. 1(c)): Despite its triangular pattern, this is the simple chain (Fig. 1(a)) extended by allowing for next nearest neighbour interactions. This lattice was motivated by the observation [25] that some models require such extensions in one dimensions to prevent degeneracy. Alternatively, it can be seen as the first step towards a two-dimensional triangular lattice (Fig. 3(a)). Each site has four neighbours, with boundary sites having either one or two virtual neighbours.

Futatsubishi lattice (Fig. 1(d)): In appreciation of the Kagomé lattice discussed below, “Futatsubishi” is a Japanese name, which translates to “two-diamond”, reflecting the shape of the lattice. The Futatsubishi lattice is fully contained in the Mitsubishi lattice (Fig. 3(d)) discussed below (three of them meet at every vertex), or as a suitable slice of the square lattice (Fig. 2(a)) or the jagged lattice (Fig. 2(b)). On the present lattice, each site has either two or four neighbours in the bulk and two virtual neighbours at the boundary.

### 2.2.2. Two-dimensional lattices

Square lattice (Fig. 2(a)): This is the standard square lattice, the most commonly used lattice the AMM has been studied on. Each site has four nearest neighbours. As indicated by the dashed lines in Fig. 2(a), edge sites have one virtual neighbour and corner sites have two, leading to a constant  $q_i = 4$  for all sites  $i$ .

Jagged lattice (Fig. 2(b)): This lattice is a square lat-

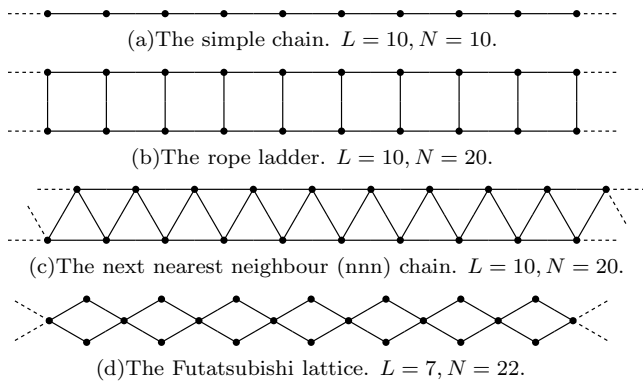


FIG. 1: The four one-dimensional lattices considered in this article. Sites are shown as filled circles, adjacency is indicated by solid lines. Dashed lines indicate links to virtual neighbours.

tice rotated by 45 degrees and fitted into a square shape which makes the boundary look jagged. The only difference to the square lattice above is therefore the boundary, where sites have either two (edge) or three (corner) virtual neighbours, producing, again, a constant  $q_i = 4$  for all sites. There are various ways of cutting the lattice out of the bulk — we decided to maintain the left-right mirror symmetry, which results in three different boundaries. In hindsight, a slightly different choice would have resulted in a lattice of higher symmetry and an aspect ratio closer to unity. The perfect match of the universal features of the AMM on this lattice with those on all others is testament of the strong universal behaviour of the model.

Archimedes lattice (Fig. 2(c)): The name of this lattice is normally complemented by  $(4, 8^2)$ , which reflects the parameters for the general rule to construct these two-dimensional lattices [26]. In the present case, every vertex is surrounded by one square and two octagons. Each lattice site in the bulk has three neighbours. Along the boundary one of them is replaced by a virtual neighbour, so that  $q_i = 3$  throughout.

Non-crossing (nc) diagonal square lattice (Fig. 2(d)): This lattice is based on a square lattice by adding alternate diagonals such that there are no crossing (nc) diagonals. Each site has either four or eight nearest neighbours. Boundary sites have either one, three or five virtual neighbours.

Triangular lattice (Fig. 3(a)): This lattice is the approximate square-shaped clipping of a tessellation of the plane by triangles. It is probably the second most frequently studied lattice in statistical mechanics. Owing to its six-fold symmetry which clashes with the four-fold symmetry of the square, boundary conditions at the upper and the lower edge differ from those on the left and on the right. This is not the case for three of the four preceding two-dimensional lattices, but does similarly apply to the following three. In the present case, the number of virtual neighbours of sites along the edge varies between

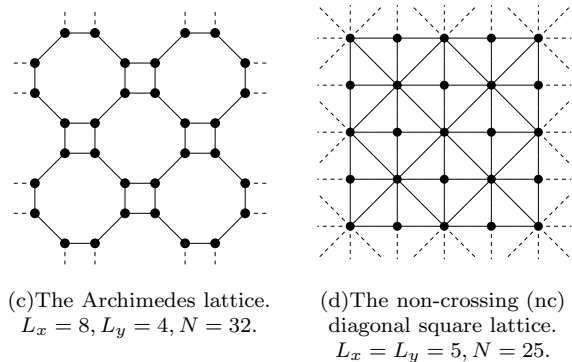
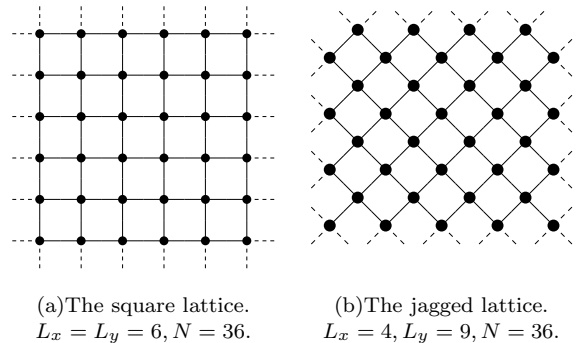


FIG. 2: The four two-dimensional lattices with four-fold symmetry considered in this article.

one and four, with a constant  $q_i = 6$  throughout.

Kagomé lattice (Fig. 3(b)): This lattice was first studied by Syôzi [12, 27]. Its name is Japanese, referring to the pattern of holes (“me”) in a basket (“kago”). Each site in the bulk has four nearest neighbours. This lattice has a six-fold symmetry, which generates three different boundary conditions by the way we decided to cut it at top and bottom. Similar to the jagged lattice (Fig. 2(b)), in hindsight we may have picked slightly different boundaries.

Honeycomb lattice (Fig. 3(c)): Similar to the triangular lattice, this lattice is a tiling by hexagons, leading to a honeycomb-shaped pattern. Each bulk site has three neighbours,  $q_i = 3$ , and the number of virtual neighbours along the edge is one everywhere, even when top and bottom edges differ from those on the left and on the right.

Mitsubishi lattice (Fig. 3(d)): This is Japanese which translates to “three-diamond” reflecting the shape of the lattice (the naming is inspired by the logo of the famous Japanese company of the same name). It is also known as “the diced lattice” [12, 27]. Each lattice site has either three or six nearest neighbours with a number of virtual neighbours at the boundary varying between one and four. Again, top and bottom edges differ from those left and right.

Some of the two-dimensional lattices are related by transforms, which are frequently used in the analysis of equilibrium critical phenomena [12, 27–29]. Denoting the

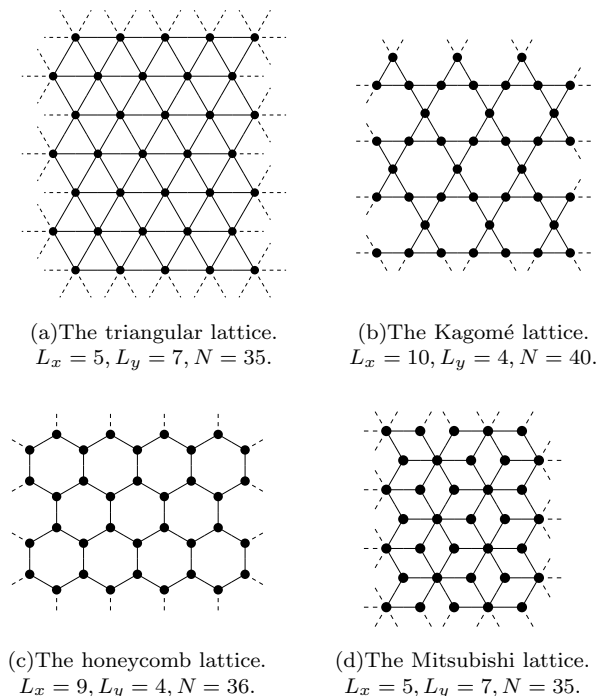


FIG. 3: The four two-dimensional lattices with six-fold symmetry considered in this article.

duality transform by  $\mathcal{D}$ , the star-triangle transform by  $\Delta$  and the decoration-iteration transform by  $\mathcal{I}$ , the following equalities hold between two-dimensional lattices:

$$\begin{aligned}
 \mathcal{D}(\text{honeycomb}) &\equiv \text{triangular} \\
 \mathcal{D}(\text{Kagomé}) &\equiv \text{Mitsubishi} \\
 \mathcal{D}(\text{Archimedes}) &\equiv \text{nc diagonal square} \\
 \mathcal{D}(\text{square}) &\equiv \text{square} \\
 \Delta(\text{Mitsubishi}) &\equiv \text{triangular} \\
 \Delta(\mathcal{I}(\text{honeycomb})) &\equiv \text{Kagomé} .
 \end{aligned}$$

### 2.3. Implementation details

Throughout this work we used the same implementation in C of the AMM, which takes as an input the adjacency information of the various lattices, that are generated separately from running the actual Manna Model. The full adjacency matrix is extremely sparse and it therefore makes little sense to store the information in that format. Rather, all sites are sequentially indexed and sites adjacent to a given site are listed by their index in a sequence (of varying length). Negative indices indicate virtual neighbours. The adjacency information is then filled into a C `struct` for each site  $i$ , which contains a vector holding the sequence of indices of adjacent sites, their number, a flag whether the site has been hit by the currently running avalanche and finally the height  $z_i$ . Using indices rather than pointers to reference sites

in our experience produces very fast code with strongly optimising compilers.

Storing the adjacency information in memory (rather than being implemented explicitly by rules), makes the code more flexible, but large lattices comparatively expensive in terms of memory requirements. Significant amounts of memory are also required for the stack of active sites, which holds every site  $i$  whose  $z_i$  exceeds 1. Sites are placed on the stack at the time when they make the transition from  $z_i = 1$  to  $z_i = 2$ . Random sequential updating requires random access to that stack. Sites  $i$  picked from the stack topple only once and thus remain on the stack until  $z_i \leq 1$ . At the time when an avalanche is triggered all sites might hold one particle, so that the theoretical maximum number of sites exceeding the threshold at any one time simultaneously is  $(N+1)/2$ . Although this maximum is not reached in practice, building in safeguards to protect smaller stacks from overflowing is computationally more costly than providing a stack as large as the theoretical maximum.

A second stack is required to keep track of all sites toppling during any one avalanche. Once a site is updated, a flag associated with it is changed, and the site's index is placed on the stack. It is an invariant that all sites with the flag raised are located on the stack. The area of an avalanche is the height of that stack at the end of the avalanche. The flags are reset by scanning through the stack.

Even when using memory lavishly, memory requirements for the AMM implementation as described above are rather modest compared to what any modern desktop computer has to offer. In one and two dimensions, large lattices are prohibitively large in terms of CPU time, not in terms of memory, as the average avalanche size grows quadratically in the linear system size, *i.e.* in the (average) chemical distance to the open (dissipative) boundary. An additional, sometimes very noticeable constraint on systems with multiple cores or multiple logical cores (hyper-threading) is the memory bus, which can be alleviated only partly by reducing the memory requirements.

### 2.4. Output

The output of the code described above is a string of moments, effectively subsamples, averaged over a number of avalanches (ranging from many millions to several ten thousand), which we call “chunks” in the following. Typically, 100 to 10 000 chunks were generated for each lattice. The statistics of the chunks allows for an estimate of the statistical error, while a simple average (weighted by the chunk size if necessary) across chunks produces an unbiased, consistent estimate of the moments.

The sizes of the chunks were chosen so that a new chunk would be produced every ten to sixty minutes. In one dimension the linear size of the lattices spanned about three orders of magnitude, in two dimensions the square root of that. The average size and thus

roughly the CPU time to produce a single avalanche grows quadratically in the linear size, ranging over six orders of magnitude in one dimension, and over three in two dimensions, see Tables I and II. The chunk sizes have to be adjusted accordingly. At the same time, the avalanche-avalanche correlation time increases like a power of the linear extension, but *not* with the dynamical exponents  $z$ , which defines the link between microscopic and macroscopic time scale, but with  $L^{D-d}$ , which is a measure of the characteristic fluctuations of the AMM in the interface picture [30–32].

The chunks were generated on the SCAN facility at Imperial College London, which harvests CPU time from undergraduate computing facilities when not used by students, providing up to 706 logical CPUs simultaneously, mostly in the form of Intel<sup>®</sup> Core2<sup>™</sup> processors with 2.66 GHz. In this setup, all I/O is done over the network, which in principle constraints the amount of output per process running. Given the drastic difference in CPU time required to generate a single avalanche, by far the most CPUs were assigned to the largest systems. In two dimensions, the smallest four system sizes each had one logical CPU to themselves. As a result, the smallest systems (that we kept, see below) have sample sizes exceeding  $10^9$  avalanches, which leads to highly accurate estimates for their momenta. In total, about 168 415 and 72 451 hours of CPU time were spent on generating the data in one and two dimension, respectively.

For simplicity, checkpointing was implemented only right after a chunk was written out. The power cycling of the computer setup thus limited the amount of time available to generate a single chunk. While the original intention was to choose the chunk size such that correlations (which normally come in the form of anti-correlations) are negligibly small, this turned out to be unsustainable for the very large system sizes. However, uncorrelated chunks greatly facilitate the calculation of statistical errors, compared to, say, a full-blown resampling plan [33]. To this end, chunks were merged during post-processing, as discussed below.

As each instance of the AMM was started with an empty lattice, a generous amount of chunks was dropped as transient from the set considered in the subsequent data analysis. This equilibration “time” was estimated by inspection of individual series of chunks, as a multiple of the time to “obvious” stationary. For the largest lattices in one dimension typically  $10^5$  avalanches (more for larger lattices) were rejected as transient and  $10^6$  retained for statistics in one dimension. In two dimensions, typical numbers were  $6 \cdot 10^6$  as transient and  $400 \cdot 10^6$  for statistics[69]. As a rule of thumb, at least 3/2 times the number of sites in the lattice avalanches were removed as transient. For smaller lattices a much larger fraction was taken, as for them, equilibration was often apparently reached within a single chunk. Equilibration can also be observed in the density of particles, which, at least in one dimension, initially grows almost perfectly linearly with only a minute amount of dissipation. Once a cer-

tain fraction of sites is occupied, the occupation density displays very little relative fluctuations, for large lattices of around  $2 \cdot 10^{-4}$ .

The transient serves the additional purpose of warming up the random number generator (RNG), which was of course seeded uniquely in each instance, except for the Mitsubishi lattice, whose 190 different seeds equal those used for honeycomb lattice. All results presented in the following are based on the Mersenne twister [34], which has received some criticism for its correlations across differently seeded instances [35]. The independence of the present results from the RNG was tested by re-running a few setups with Marsaglia’s KISS RNG [36].

## 2.5. Statistical error

All results presented below are based on moments of the avalanche size, area and duration.

The first moments of all three observables generally posed a problem, possibly because they were determined with an accuracy so high that it was virtually impossible to account for their corrections to scaling (see below). The statistical error of all moments was calculated on the basis of chunks whose size was chosen as to ensure their independence. This was tested by firstly calculating their autocorrelation function and, secondly, by successively increasing their size, *i.e.* merging them, to probe whether the statistical error derived on their basis was affected by this operation. In fact, for the largest system sizes (and thus smallest chunk sizes) tested, some correlations were visible (correlation length of about 0.7 chunks), and we decided to merge ten consecutive chunks throughout. It turned out, however, that only the statistical errors of the first moments were noticeably, yet still insignificantly, affected at all by this operation.

It is straight-forward to determine estimates and their estimated variance on the basis of independent chunks. Denoting the observable in the  $i$ th chunk by  $c_i$ , an unbiased, consistent estimator [37] of its population average  $\langle c \rangle$  is

$$\frac{1}{M_c} \sum_{i=1}^{M_c} c_i \quad (1)$$

given a sample size of  $M_c$ . In the following, we will denote that estimate itself by  $\langle c \rangle$ . An unbiased, consistent estimator of the variance of this estimator is

$$\frac{1}{M_c - 1} \left[ \frac{1}{M_c} \sum_{i=1}^{M_c} c_i^2 - \left( \frac{1}{M_c} \sum_{i=1}^{M_c} c_i \right)^2 \right]. \quad (2)$$

These estimates were used as input values for the estimation of the exponents, based on the scaling assumption discussed in the following. For completeness, covariances of the estimators for the averages of two observables  $c$

and  $c'$ , as used in Eq. (18), were estimated using

$$\text{cov}(c, c') = \frac{1}{M_c - 1} \left[ \frac{1}{M_c} \sum_{i=1}^{M_c} c_i c'_i - \left( \frac{1}{M_c} \sum_{i=1}^{M_c} c_i \right) \left( \frac{1}{M_c} \sum_{i=1}^{M_c} c'_i \right) \right]. \quad (3)$$

As detailed below, the finite size scaling of the moments of each observable was determined in the form

$$\langle x^n \rangle = a_{x,n} L^{\mu_n^{(x)}} + \text{corrections} \quad (4)$$

where  $x$  stands for the size  $s$ , the area  $a$  or the duration  $t$ . The combined information of the scaling of a number of different moments  $n$  was then used to estimate the finite size scaling exponents. Even when we implemented the first eight moments, we used only moments 2 to 4 (e.g.  $\mu_2^{(s)}$ ,  $\mu_3^{(s)}$ ,  $\mu_4^{(s)}$ ) when fitting the avalanche dimension (using  $2 = (2 - \tau)D$  to determine  $\tau$ ) and moments 2 to 5 to fit exponents characterising the scaling of avalanche area and duration (all exponents are defined below). Different moments estimated on the basis of a single Monte-Carlo simulation are not independent. To account for that, we (rather generously) multiplied the statistical error of each moment by the square root of the number of moments considered simultaneously, as if each moment was determined independently from the others [38]. For example, the statistical error of the second, third and fourth moment of the avalanche size was multiplied by  $\sqrt{3}$ , before  $\mu_2^{(s)}$ ,  $\mu_3^{(s)}$  and  $\mu_4^{(s)}$  respectively were determined. It seems that these correlations are frequently ignored in the literature. This procedure does *not* account for correlations in the estimates of moments of different observables and thus our results for the finite size scaling exponents for different observables are not independent. Multiplying again by the square root of the number of different observables considered, may, however, seriously overestimate the impact of these correlations.

## 2.6. Finite size scaling

Making the usual finite size scaling assumption for observable  $x$ , its probability density function  $\mathcal{P}^{(x)}(x)$  follows

$$\mathcal{P}^{(x)}(x; L) = a_x x^{-\tau_x} \mathcal{G}_x \left( \frac{x}{b_x L^{D_x}} \right) \quad (5)$$

asymptotically in large  $x \gg x_0$  with lower cutoff  $x_0$ , linear system size  $L$ , non-universal metric factors  $a_x$  and  $b_x$  and universal exponents  $\tau_x$  and  $D_x$ . Below, the fractal dimension of avalanches is denoted by  $D_a$  [39] and the avalanche area exponent by  $\tau_a$ . For historic reasons, the dynamical exponent is denoted by  $z$  (rather than  $D_t$ ), the avalanche duration exponent by  $\alpha$  (rather than  $\tau_t$ ), and finally the avalanche dimension by  $D$  (rather than

$D_s$ ) and the avalanche size exponent by  $\tau$  (rather than  $\tau_s$ ). The universal, dimensionless scaling function  $\mathcal{G}_x$  of a dimensionless argument decays, for large arguments, faster than any power law, so that all moments

$$\langle x^n \rangle(L) = \int_0^\infty dx \mathcal{P}^{(x)}(x; L) x^n \quad (6)$$

exist for any finite system and  $n \geq 0$ . Provided that  $n + 1 - \tau > 0$  one can easily show [40, 41] that gap scaling follows, so that

$$\langle x^n \rangle(L) = a_x (b_x L^{D_x})^{n+1-\tau_x} \int_0^\infty dy y^{n-\tau_x} \mathcal{G}_x(y) \quad (7)$$

asymptotically in large  $L$ , or, more accurately,

$$0 < \lim_{L \rightarrow \infty} \frac{\langle x^n \rangle(L)}{L^{D_x(n+1-\tau_x)}} < \infty. \quad (8)$$

To determine  $D_x$  (and  $\tau_x$ , if independent), the leading order scaling of the moments according to Eq. (4) was estimated, fitting the resulting exponents  $\mu_n^{(x)}$  against  $D_x(n + 1 - \tau_x)$ , without allowing for any further corrections. The results are shown in Tables III and IV.

Because of particle conservation in the bulk, every particle placed on the lattice anywhere can only leave through the boundary. On the way there, it performs an independent random walk, even when it occasionally rests [3]. Every move by a particle is caused by a site's toppling and the number of particle moves during an avalanche is therefore exactly twice the number of topplings. At stationarity one particle leaves the system per particle added and (half) its trajectory length is its contribution to the various avalanches it has been part of. The average contribution per particle and thus per avalanche is the average trajectory length, which scales like  $L^2$  independent of the dimensionality of the lattice [13] and many of the details of the boundary. This argument remains valid if avalanches of size 0 are excluded from the average (which we did *not*), provided the probability of producing an avalanche of size 0 (i.e. hitting an empty site) does not converge to 1.

As a result  $\langle s \rangle \propto L^2$  asymptotically, or, here,  $\langle s \rangle \propto N^{2/d}$ , i.e.  $\mu_1^{(s)} = 2$  and under the assumption of gap scaling  $2 = (2 - \tau)D$ . This identity has been used in the fitting of the avalanche dimension, i.e.  $\mu_n^{(s)}$  for  $n = 2, 3, 4$  was fitted against  $2 + D(n - 1)$ . At the same time, comparing the estimate for  $\mu_1^{(s)}$  (Tables III and IV) to the exact value 2 allowed us to assess the fitting procedure, in particular the form of the corrections discussed below.

Defining

$$-\Sigma_x = D_x(\tau_x - 1) \quad (9)$$

the assumption of a sufficiently [42, 43] narrow joint probability density function [39, 44, 45] produces the scaling law  $\Sigma := \Sigma_s = \Sigma_t = \Sigma_a$ , i.e.

$$-\Sigma = D(\tau - 1) = z(\alpha - 1) = D_a(\tau_a - 1). \quad (10)$$

As this is not a mathematical identity [30] (in fact, it seems to be broken in the original Manna Model [39]) it is tested as a scaling hypothesis below. The exponent  $\Sigma$  can be seen as a replacement for the exponents  $\tau$ ,  $\alpha$  and  $\tau_a$ , as  $\mu_n^{(s)} = nD + \Sigma$ ,  $\mu_n^{(t)} = nz + \Sigma$ ,  $\mu_n^{(a)} = nD_a + \Sigma$  for  $n > \tau - 1$ ,  $n > \alpha - 1$  and  $n > \tau_a - 1$  respectively.

Finally, as in the BTW model [46], in the Manna Model avalanches are often assumed to be compact [4, 42], *i.e.*  $D_a = d$  (supposedly up to the upper critical dimension, where we expect dangerous irrelevant fields to spoil this scaling relation). There is no mathematical proof for this feature, yet numerically it is well verified, see Tables III and IV. Clearly  $D_a \leq d$ , which served as another constraint to assess the quality of the exponents extracted.

### 2.6.1. Corrections to scaling

The exponents  $\mu_n^{(x)}$  characterise the asymptotic scaling of the moments in large  $L$ . It is widely known [47], however, finite lattices suffer from finite size corrections, which manifest themselves as sub-leading terms to be included on the right hand side of Eq. (4) [42]. A priori, the structure of the corrections is not known, yet they have a marked impact on the quality of the results, as they are *imposed* when fitting the data.

Given that there is often no natural way of defining the linear extent of a lattice, we decided to replace  $L$  (as in Eq. (4)) by  $N^{1/d}$ . We considered a host of different fitting functions, such as

$$\langle x^n \rangle (N) = A_{x,n} N^{\mu_n^{(x)}/d} \quad (11)$$

$$\langle x^n \rangle (N) = A_{x,n} N^{\mu_n^{(x)}/d} + B_{x,n} N^{\mu_n^{(x)}/d - \omega_{x,n}/d} \quad (12)$$

$$\langle x^n \rangle (N) = A_{x,n} N^{\mu_n^{(x)}/d} + B_{x,n} N^{\mu_n^{(x)}/d - 1/4} \quad (13)$$

$$\langle x^n \rangle (N) = A_{x,n} N^{\mu_n^{(x)}/d} + B_{x,n} N^{\mu_n^{(x)}/d - 1/2} + C_{x,n} N^{\mu_n^{(x)}/d - 1} \quad (14)$$

and eventually settled for

$$\langle x^n \rangle (N) = A_{x,n} N^{\mu_n^{(x)}/d} + B_{x,n} N^{\mu_n^{(x)}/d - 1/4} + C_{x,n} N^{\mu_n^{(x)}/d - 1/2} \quad (15)$$

which yielded particularly good estimates. In particular,  $\mu_1^{(s)} = 2$  was reproduced quite reliably. The quality of the estimates was assessed on the basis of the goodness of fit determined in the Levenberg-Marquardt least square fitting routine [48]. For the vast majority of moments and lattices, we could have dropped the last term in Eq. (15) arriving Eq. (13) and still achieved a goodness of fit ( $q$ -value) of more than 0.9. However, the first moments of the avalanche size, whose finite size scaling exponent is the only exactly known one, was particularly poorly fitted without that term. For consistency, we decided to fit *all* moments using Eq. (15), achieving typically  $q$ -values of better than 0.9, suggesting that we overestimated the

statistical errors. In all result tables, fits that had a  $q$ -value of less than 0.1 are marked as such.

To reduce the impact of a possible dependence on the (arbitrary) choice of the initial values of the free parameters, the number of terms in the fitting function was increased successively starting from Eq. (11), using the estimates of the parameters in the previous fit as the initial value of the same parameters in the next.

The simplicity of Eq. (15) meant that we had to drop results for small system sizes, which suffer from stronger finite size corrections, yet were determined with much greater accuracy than those of the bigger systems. This is a common theme in the present work: Moments in small system sizes were determined with such great accuracy that very many (a priori unknown) correction terms would have to be included to account for all such details. At the same time, it makes little sense to have almost as many free parameters in the fitting function as there are data points to fit. In order to retain the goodness of fit as a meaningful device to determine the quality of the fit, we therefore removed the smallest four system sizes from the procedure (in one and two dimensions), keeping the seven system sizes listed in Tables I and II.

Increasing the system size in order to suppress correction terms comes at the price of increased relative error if  $\tau_x > 1$ . According to Eq. (4) and Eq. (8), the variance of the  $n$ th moment has leading order  $L^{D_x(2n+1-\tau_x)}$ , *i.e.* the relative error scales like  $L^{D_x(\tau_x-1)/2}$ . Moreover, correlations are expected to die off after  $L^{D-d}$ , which reduces the number of effectively independent measurements with increasing system size.

### 2.7. Moment ratios

Ratios of products of moments, which (to leading order) are independent from  $L$ , characterise the scaling function  $\mathcal{G}_x$ , Eq. (5), directly. In equilibrium phase transition, the so-called Binder-cumulant [49, 50] is the best known such ratio, signalling the deviation from a Gaussian distribution of the order parameter around the critical point. There are many ways of constructing suitable moment ratios; assuming  $\langle x^n \rangle \propto L^{D_x(n+1-\tau_x)}$ , it is easy to see that any ratio of products of moments, which has the same number of moments (to cancel  $\tau_x \neq 1$ ) and the same sum of orders of moments (to cancel  $D_x$ ) in numerator and denominator leads to a non-scaling quantity. Since the second moment is positive and bounded away from 0, traditionally moment ratios are formed by dividing by a power of it. Moreover, in many phase transitions, the order parameter follows a distribution with  $\tau_x = 1$ , which removes the constraint of having the same number of moments in the numerator and the denominator.

While the sets  $\langle x^{n-m} \rangle \langle x^{n+m} \rangle / \langle x^n \rangle^2$  attracts by its

simplicity and symmetry, the set

$$g_n^{(x)} = \frac{\langle x^n \rangle \langle x \rangle^{n-2}}{\langle x^2 \rangle^{n-1}}, \quad (16)$$

has the particularly nice feature that  $g_1^{(x)} = g_2^{(x)} = 1$  by definition, which fixes the metric factors  $a_x$  and  $b_x$  in Eq. (5) by *imposing* for  $n = 1, 2$

$$g_n^{(x)} = \int_0^\infty dy y^{n-\tau_x} \mathcal{G}_x(y), \quad (17)$$

see Eq. (7) which is then consistent with Eq. (16) for all  $n$ .

The statistical error  $\sigma(g_n^{(x)})$  of the estimator of Eq. (16) is to leading order in the sample size given by

$$\begin{aligned} \sigma^2(g_n^{(x)}) = & (g_n^{(x)})^2 \left( \frac{\text{cov}(x^n, x^n)}{(\langle x^n \rangle)^2} + (n-2)^2 \frac{\text{cov}(x^1, x^1)}{(\langle x \rangle)^2} + (n-1)^2 \frac{\text{cov}(x^2, x^2)}{(\langle x^2 \rangle)^2} \right. \\ & \left. - 2(n-2)(n-1) \frac{\text{cov}(x^2, x^1)}{\langle x \rangle \langle x^2 \rangle} - 2(n-1) \frac{\text{cov}(x^2, x^n)}{\langle x^2 \rangle \langle x^n \rangle} + 2(n-2) \frac{\text{cov}(x^1, x^n)}{\langle x \rangle \langle x^n \rangle} \right), \quad (18) \end{aligned}$$

which matches perfectly (typically the first three or four significant digits) the error as found by the subsampling using chunks, *i.e.* determining  $g_n^{(x)}$  for each chunk and estimating the error by the square root of its variance over the number of chunks. In Eq. (18)  $\langle x^n \rangle$  strictly denotes the *estimator* of the  $n$ th moment and  $\text{cov}(x^n, x^m)$  the estimated covariance of the  $n$ th and  $m$ th moment, see Eq. (3). Consistent with the preceding discussion, we used averages and statistical errors derived from chunks.

All lattices were set up with the intention of creating an aspect ratio of 1, which is trivial as long as the lattice has a four-fold symmetry. In particular for lattices without that symmetry, such as the triangular lattice (Fig. 3(a)), the Kagomé lattice (Fig. 3(b)), the honeycomb lattice (Fig. 3(c)) and the Mitsubishi lattice (Fig. 3(d)), but also, say, the jagged lattice (Fig. 2(b)), the aspect ratio might deviate slightly from unity and converge to 1 only with increasing system size. In any case, the aspect ratio might be more reasonably be defined using the Manhattan distance across the lattice. It is well known that universal scaling exponents are generally independent from the aspect ratio, whereas finite size scaling functions are not [51]. Therefore, deviations of the moment ratios in particular in case of the lattices listed above are expected (but did in fact not materialise). Surprisingly, even when there is every reason to assume that no such problem can occur in one dimension, their moment ratios proved particularly difficult to analyse.

### 3. RESULTS

#### 3.1. Avalanche exponents

After stripping off the transient, merging chunks as discussed above, deriving average moments and errors using the procedures described above, the scaling exponents  $\mu_n^{(x)}$  were fitted using Eq. (15) for the three different observables,  $x = s, t, a$ , avalanche size, duration and area respectively. As mentioned above, correlations between moments were taken into account by multiplying the statistical error of the moment by the square root of the number of moments considered. Allowing for no further corrections,  $\mu_n^{(s)}$  were fitted for each of the twelve different lattices separately against

$$\mu_n^{(s)} = 2 + D(n-1) \quad (19)$$

for  $n = 2, 3, 4$ . The results are collected in Table III. The scaling law  $2 = (2 - \tau)D$  used in Eq. (19) was probed independently;  $\mu_1^{(s)} = 2$  is a mathematical identity, but valid only *asymptotically* and the deviation of  $\mu_1^{(s)}$  from 2 can therefore serve as an indicator to assess the quality of the fitting routines and the data and can help confirming that “asymptotia is reached”. The estimate for  $\mu_1^{(s)}$  on the basis of Eq. (15) is shown in Table III alongside the other finite size scaling exponents. The exponent  $\tau$  stated in Table III is derived from the estimate of  $D$  using  $\tau = 2 - 2/D$ .

For all observables (size, area and duration), the first moments turned out to be problematic. According to Eq. (6) moments  $n < \tau - 1$  remain finite in the thermodynamic limit, consistent with our observation that smaller moments generally require more correction terms.

The average avalanche size is particularly difficult to handle, which is determined, due to the presence of anti-correlations [31, 32], with incredible precision, typically with a relative error of the order  $10^{-5}$ . We therefore decided to omit first moments from the determination of the finite size scaling exponents throughout.

For  $x = t$  and  $x = a$  no scaling laws were used (even when  $D_a = d$  is generally assumed to hold) and so the exponents  $\mu_n^{(x)}$  were fitted against:

$$\mu_n^{(t)} = z(n + 1 - \alpha) \quad (20)$$

$$\mu_n^{(a)} = D_a(n + 1 - \tau_a) \quad (21)$$

for  $n = 2, 3, 4, 5$ .

Fitting moments beyond  $n = 5$  proved very difficult. We decided to drop all moments beyond the fourth for avalanche size and beyond the fifth for the avalanche area and duration, as  $\mu_n^{(x)}$  became clearly dependent on the choice of the initial values of the fitting parameters. As mentioned above, in all fitting schemes used, we increased the number of free parameters successively and used the estimates of the fitting parameters of one scheme as the initial values for its extension. For example, we used  $A_{x,n}$  and  $\mu_n^{(x)}/d$  from a fit against Eq. (11) as initial values in a fit against Eq. (13), which in turn produced the initial values of  $A_{x,n}$ ,  $B_{x,n}$  and  $\mu_n^{(x)}/d$  to fit with Eq. (15). We observed this procedure in all fitting schemes discussed below.

As the variance of the  $n$ th moment scales like  $L^{D_x(2n+1-\tau_x)}$ , its numerical estimate is increasingly affected by the floating point precision (double-extended throughout) — equivalently, the typical largest measurement of the  $n$ th moment scales like the  $n$ th power of the cutoff,  $L^{nD_x}$ , which for  $n = 6$ ,  $D_x = 2.25$  and  $L = 2^{16}$  is  $2^{216}$ . Given that the smallest event size is 0, this is to be compared to the 64 bits in the mantissa on a `long double` on the x86 architecture.

The exponent  $\Sigma_x$  can be derived either from the definition Eq. (9) through  $D_x$  and  $\tau_x$  or by independently fitting  $\mu_n^{(x)}$  against  $nD_x + \Sigma_x$ . We took that approach for  $x = t$  and  $x = a$ . Using the three different observables size, duration and area, provides effectively estimates for  $D(\tau - 1)$ ,  $z(\alpha - 1)$  and  $D_a(\tau_a - 1)$  respectively. In the case of  $D(\tau - 1)$  this is in fact exactly  $D - 2$ , since we imposed  $D(2 - \tau) = 2$  when estimating  $D$ . The entry for  $\Sigma_s$  in Table III is therefore derived from the estimate for  $D$ . Except for  $\tau$ , all other entries in Table III are based on fitting  $\mu_n^{(x)}$  directly.

Table III provides very strong support for universality across different lattices. Under the assumption that universality holds, estimates for exponents gained from different lattices can be taken together to produce an overall estimate. The result of that procedure is shown in Table IV. As discussed further below, we regard only the data referring to the fitting function Eq. (15), shown in bold, as reliable, producing the most consistent and robust results.

Fits with Eq. (15) produced very large  $q$ -factors, suggesting we had been too generous either with estimating the statistical errors or with the number of free parameters. We therefore also tried Eq. (13), which, however, gave partly inconsistent results. In particular estimates for  $\mu_1^{(s)}$  deviated from the exact value 2 by about 30 standard deviations (although the relative error was only  $3 \cdot 10^{-3}$ ). For the simple chain the avalanche size moments tested displayed a poor quality of fit using Eq. (13), as did the first moments of the avalanche size for all lattices except for the nnn chain (Fig. 1(c)), the Futatsubishi lattice (Fig. 1(d)) and the Archimedes lattice (Fig. 2(c)). The results for the fits against Eq. (13) are also summarised in Table IV. A bracket [·] indicates finite size scaling exponents not being fitted with a goodness of fit better than 0.1.

In general, the Futatsubishi lattice and the simple chain were particularly difficult to fit using whichever fitting function.

In order to extract the exponent of the sub-leading terms, the remainder  $\langle x^n \rangle(N) - A_{x,n}N^{\mu_n^{(x)}/d}$  was fitted against

$$\tilde{B}_{x,n}N^{\mu_n^{(x)}/d - \omega_{x,n}/d} \quad (22)$$

determining  $\omega_{x,n}$ . This procedure was aiming much more at a qualitative result rather than a quantitative one and generated rather noisy estimates. The Futatsubishi and the triangular lattices proved particularly difficult to handle. The data in  $d = 1$  produced, unfortunately quite inconsistently  $\omega_{s,n} \approx 0.28$ ,  $\omega_{t,n} \approx 0.20$  and  $\omega_{a,n} \approx 0.20$ , while  $d = 2$  produced, slightly more consistently  $\omega_{s,n} \approx 0.23$ ,  $\omega_{t,n} \approx 0.32$  and  $\omega_{a,n} \approx 0.47$  fairly independent of lattice and  $n$  (but more reliably for large  $n$  and observables other than the avalanche size). These exponents could in turn be used in Eq. (12) to fit the data for  $\mu_n^{(x)}$  at fixed  $\omega_{x,n}$ . The resulting overall estimates for the finite size scaling exponents are also shown in Table IV.

### 3.2. Moment ratios

Similar to the plain moments, one has to allow for corrections when fitting moment ratios. Most two-dimensional lattices (except nc diagonal square lattice (Fig. 2(d)) and Mitsubishi lattice (Fig. 3(d))) produced consistent results with a goodness of fit of greater than 0.1 with

$$g_n^{(x)} + D_{x,n}N^{-0.25} \quad (23)$$

but in order to capture all lattices and for consistency with the above we decided to add a further correction, finally fitting against

$$g_n^{(x)} + D_{x,n}N^{-0.25} + E_{x,n}N^{-0.5} \quad (24)$$

In contrast to the finite size scaling exponents  $\mu_n^{(x)}$  of the moments considered above, all moment ratios were

TABLE III: Summary of all exponents characterising the avalanching in the twelve different lattices, using Eq. (15). The estimates for  $\tau$  and  $D(\tau - 1)$  were *not* determined by fitting the data, but through the scaling relation  $D(2 - \tau) = 2$ . The estimates for  $\mu_1^{(s)}$  verify this scaling relation. The estimates in the last three columns should coincide under the narrow-joint-distribution assumption, Eq. (10). Estimates for different observables are *not* independent.

lattice	$d$	$D$	$\tau$	$z$	$\alpha$	$D_a$	$\tau_a$	$\mu_1^{(s)}$	$-\Sigma_s$	$-\Sigma_t$	$-\Sigma_a$
Simple chain	1	2.27(2)	1.117(8)	1.450(12)	1.19(2)	0.998(4)	1.260(13)	2.000(4)	0.27(2)	0.27(3)	0.259(14)
Rope ladder	1	2.24(2)	1.108(9)	1.44(2)	1.18(3)	0.998(7)	1.26(2)	1.989(5)	0.24(2)	0.26(5)	0.26(2)
nnn chain	1	2.33(11)	1.14(4)	1.48(11)	1.22(14)	0.997(15)	1.27(5)	1.991(11)	0.33(11)	0.3(2)	0.27(5)
Futatsubishi	1	2.24(3)	1.105(14)	1.43(3)	1.16(6)	0.999(15)	1.24(5)	2.008(11)	0.24(3)	0.23(9)	0.24(5)
Square	2	2.748(13)	1.272(3)	1.52(2)	1.48(2)	1.992(8)	1.380(8)	1.9975(11)	0.748(13)	0.73(4)	0.76(2)
Jagged	2	2.764(15)	1.276(4)	1.54(2)	1.49(3)	1.995(7)	1.384(8)	2.0007(12)	0.764(15)	0.76(5)	0.77(2)
Archimedes	2	2.76(2)	1.275(6)	1.54(3)	1.50(3)	1.997(10)	1.382(11)	2.001(2)	0.76(2)	0.78(6)	0.76(3)
nc diagonal square	2	2.750(14)	1.273(4)	1.53(2)	1.49(2)	1.992(7)	1.381(8)	2.0005(12)	0.750(14)	0.75(4)	0.76(2)
Triangular	2	2.76(2)	1.275(5)	1.51(2)	1.47(3)	2.003(11)	1.388(12)	1.997(2)	0.76(2)	0.71(6)	0.78(3)
Kagomé	2	2.741(13)	1.270(4)	1.53(2)	1.49(2)	1.993(8)	1.381(9)	1.9994(12)	0.741(13)	0.75(5)	0.76(2)
Honeycomb	2	2.73(2)	1.268(6)	1.55(4)	1.51(4)	1.990(13)	1.376(14)	2.000(2)	0.73(2)	0.79(8)	0.75(3)
Mitsubishi	2	2.75(2)	1.273(6)	1.54(3)	1.50(4)	1.999(12)	1.387(12)	1.998(2)	0.75(2)	0.77(7)	0.77(3)

TABLE IV: Overall estimates of scaling exponents in one and two dimensions. Only the fits using Eq. (15), based on the data in Table III and shown in bold, are fully reliable. Entries for Eq. (13) and Eq. (12) are for comparison to other estimates only. Fits with a goodness of less than 0.1 are marked by [.]. The estimate for  $\Sigma$ , Eq. (10), is based on all estimates for  $D(\tau - 1)$ ,  $z(\alpha - 1)$  and  $D_a(\tau_a - 1)$  in Table III. Their correlation is taken into account by multiplying their respective error by  $\sqrt{3}$ .

$d$	function	$D$	$\tau$	$z$	$\alpha$	$D_a$	$\tau_a$	$-\Sigma$
1	<b>Eq. (15)</b>	<b>2.253(14)</b>	<b>1.112(6)</b>	<b>1.445(10)</b>	<b>1.18(2)</b>	<b>0.998(3)</b>	<b>1.259(11)</b>	<b>0.26(2)</b>
1	Eq. (13)	[2.265(4)]	[1.117(2)]	[1.449(2)]	1.172(3)	1.0000(6)	1.249(2)	0.249(3)
1	Eq. (12)	[2.2520(3)]	[1.11188(11)]	[1.4632(6)]	[1.219(2)]	1.0000(8)	1.276(2)	[0.297(3)]
2	<b>Eq. (15)</b>	<b>2.750(6)</b>	<b>1.273(2)</b>	<b>1.532(8)</b>	<b>1.4896(96)</b>	<b>1.995(3)</b>	<b>1.382(3)</b>	<b>0.761(13)</b>
2	Eq. (13)	2.7698(12)	1.2779(3)	1.5407(14)	1.498(2)	1.9990(5)	1.3843(6)	0.768(2)
2	Eq. (12)	[2.7673(3)]	[1.27728(7)]	1.541(2)	1.501(2)	1.9985(6)	1.3853(6)	0.770(2)

fitted as if they were independent, *i.e.* considering them simultaneously may be misleading as they are correlated and these correlations have not been accounted for.

The results are shown in Table V. In general, two dimensional lattices are much better than one dimensional ones. The observable most easily fitted is the area size distribution (which might be caused by the plain amplitudes  $A_{a,n}$  being universal, see below). The only two-dimensional lattice that displayed low goodness of fit throughout was the triangular lattice, while the honeycomb lattice had a single poorly fitting ratio. In one dimension, the picture is reversed; There is hardly any reasonably fittable moment ratio. Fits which produced a goodness of less than 0.1 are marked in Table V again by [.]. Results are rather noisy for the highest moment ratios, which might suggest an explanation for the slight inconsistencies, which are not covered by the statistical error, for example for  $g_6^{(a)}$  in nc diagonal square lattice (Fig. 2(d)) and Mitsubishi lattice (Fig. 3(d)). Yet, in one dimension, it is the lower order moment ratios that were most difficult to handle.

The overall estimates for the moment ratios are shown in Table VI. We refrained from stating an overall esti-

mate, where not at least two lattices produced reliable estimates as shown in Table V. Those that show low quality of fit are marked as above.

There is, again, a certain sensitivity to the fitting function; Eq. (23) gives slightly incompatible results, with remarkably small error bars. Given what has been said about the goodness of fit, we place our confidence in the results presented in Table VI.

#### 4. DISCUSSION

Exponents (Table III) and, at least in two dimensions, moment ratios (Table V) are universal across different lattices. Subleading orders of moments are noisy, but still fairly consistent. There can be little doubt that the Abelian Manna model displays all the hallmarks of a critical system as they are known from equilibrium critical phenomena. The exponents shown in bold in Table IV and the moment ratios in Table VI (except those shown in brackets) are perfectly consistent across all our results and represent reliable, high accuracy estimates of the universal quantities characterising this universality class.

TABLE V: Estimates for the moment ratios as defined in Eq. (16) obtained by fitting the relevant ratios against Eq. (24). Fits with a goodness of less than 0.1 are marked by [·].

lattice	$d$	$x$	$g_3^{(x)}$	$g_4^{(x)}$	$g_5^{(x)}$	$g_6^{(x)}$
Simple chain	1	<i>s</i>	[1.482(4)]	[2.68(2)]	[5.40(11)]	[11.3(5)]
Rope ladder	1	<i>s</i>	[1.453(6)]	[2.48(3)]	[4.43(15)]	[7.2(6)]
nnn chain	1	<i>s</i>	[1.479(13)]	[2.61(7)]	[5.0(3)]	[9.4(13)]
Futatsubishi	1	<i>s</i>	[1.412(10)]	[2.26(6)]	[3.5(2)]	[3.58(97)]
Square	2	<i>s</i>	1.825(3)	4.35(2)	12.25(14)	39.0(8)
Jagged	2	<i>s</i>	1.830(3)	4.38(2)	12.44(14)	39.9(8)
Archimedes	2	<i>s</i>	1.821(4)	4.32(3)	12.1(2)	37.86(99)
nc diagonal square	2	<i>s</i>	1.828(3)	4.36(2)	12.30(14)	39.2(8)
Triangular	2	<i>s</i>	[1.830(5)]	[4.37(3)]	[12.3(2)]	[39.1(11)]
Kagomé	2	<i>s</i>	1.832(3)	4.40(3)	12.6(2)	40.9(9)
Honeycomb	2	<i>s</i>	1.829(5)	4.38(4)	12.5(2)	40.2(11)
Mitsubishi	2	<i>s</i>	1.820(5)	4.31(4)	12.0(2)	37.4(11)
Simple chain	1	<i>t</i>	[1.472(3)]	[2.63(2)]	[5.34(7)]	[11.9(3)]
Rope ladder	1	<i>t</i>	[1.455(4)]	[2.52(2)]	[4.84(9)]	[9.8(4)]
nnn chain	1	<i>t</i>	[1.470(9)]	[2.58(5)]	[5.0(2)]	10.3(8)
Futatsubishi	1	<i>t</i>	[1.437(6)]	[2.43(3)]	[4.44(13)]	[8.2(5)]
Square	2	<i>t</i>	2.116(2)	5.95(2)	19.90(13)	75.7(9)
Jagged	2	<i>t</i>	2.117(2)	5.96(2)	20.06(13)	77.0(9)
Archimedes	2	<i>t</i>	2.115(3)	5.94(2)	19.9(2)	76.1(11)
nc diagonal square	2	<i>t</i>	2.114(2)	5.93(2)	19.78(13)	74.9(9)
Triangular	2	<i>t</i>	2.113(4)	[5.93(3)]	[19.8(2)]	[75.0(13)]
Kagomé	2	<i>t</i>	2.116(3)	5.96(2)	20.04(14)	76.95(96)
Honeycomb	2	<i>t</i>	2.110(4)	5.89(3)	19.6(2)	74.4(12)
Mitsubishi	2	<i>t</i>	2.110(3)	5.90(3)	19.7(2)	74.8(12)
Simple chain	1	<i>a</i>	1.3318(6)	1.961(2)	3.037(5)	4.839(11)
Rope ladder	1	<i>a</i>	1.3301(11)	1.957(4)	3.029(9)	4.83(2)
nnn chain	1	<i>a</i>	1.340(2)	[1.990(7)]	[3.11(2)]	[5.00(4)]
Futatsubishi	1	<i>a</i>	1.332(2)	1.962(6)	3.038(15)	4.85(3)
Square	2	<i>a</i>	1.7501(11)	3.709(5)	8.69(2)	21.66(7)
Jagged	2	<i>a</i>	1.7496(10)	3.710(5)	8.70(2)	21.72(7)
Archimedes	2	<i>a</i>	1.7503(14)	3.712(7)	8.70(3)	21.711(98)
nc diagonal square	2	<i>a</i>	1.7517(10)	3.718(5)	8.72(2)	21.78(7)
Triangular	2	<i>a</i>	1.749(2)	3.710(8)	8.70(3)	21.73(11)
Kagomé	2	<i>a</i>	1.7500(10)	3.713(5)	8.71(2)	21.78(7)
Honeycomb	2	<i>a</i>	[1.747(2)]	3.698(9)	8.66(3)	21.62(11)
Mitsubishi	2	<i>a</i>	1.748(2)	3.703(8)	8.67(3)	21.62(11)

In the literature can be found a large number of estimates for the exponents in Table IV. Traditionally, the AMM is studied in two dimensions and therefore many more estimates are available in that dimension. Given that the AMM is in the same universality class as the Oslo Model [3, 15], there is a second source for comparison. What makes the comparison more complicated is the fact that many authors have studied variants of the Manna Model (in fact, the Abelian version studied here is a variant of the original model); for example Dickman and Campelo studied the Manna Model with

height restrictions [20] and Lübeck and Heger studied its “fixed energy sandpile” version [56, 60]. Table VII collects a broad range of estimates across the literature, which nevertheless provide a perfectly consistent picture. The present work clearly improves on comprehensiveness and on accuracy, which for most estimates is improved by one digit. The fact that some estimates in the literature have even smaller error bars than ours might be partly due to our over-estimation of statistical errors but also due to other authors using models that are better behaved in one dimension, as in [52, 53].

TABLE VI: Overall estimates for the moment ratios defined in Eq. (16), based on the data presented in Table V, if enough data was available.

$d \times$	$g_3^{(x)}$	$g_4^{(x)}$	$g_5^{(x)}$	$g_6^{(x)}$
1 s	—	—	—	—
1 t	—	—	—	—
1 a	[1.3320(5)]	1.961(2)	3.035(4)	4.838(9)
2 s	1.8273(14)	4.363(10)	12.32(6)	[39.3(3)]
2 t	2.11423(98)	5.939(8)	19.88(6)	75.8(4)
2 a	1.7501(4)	3.711(2)	8.699(8)	21.72(3)

Table VII also contains the avalanche exponents for the directed percolation (DP) universality class. The exponent  $D$  is derived through the identity  $D = d + z - \beta/\nu_\perp$ , where  $-\beta/\nu_\perp$  is the finite size scaling exponent of the activity in DP [70]. The dynamical exponent  $z$  is sometimes used in the DP literature as what would have been in the present notation  $2/z$ . The exponent for  $D_a$  is based on the assumption of compact avalanches [55]. Although sometimes disputed in the literature [61, 62] using avalanche exponents leaves little doubt that the Manna universality class differs from DP. As DP is normally performed with periodic boundaries and with different observables, there is, to our knowledge unfortunately no published work on the moment ratios we considered here. In fact, depending on the definition of the ensemble [56, 63–65], some moment ratios in DP can be undefined.

Certain finite size scaling features specific to SOC are confirmed as well: Compactness of avalanches,  $D_a = d$  is very strongly supported (in two dimensions the deviation of  $D_a$  from  $d$  is slightly bigger than one standard deviation, though), as is the universality of  $\Sigma$ , Eq. (9). It is reassuring that the asymptotics of the first moment of the avalanche size,  $\mu_1^{(s)} = 2$ , are recovered, validating our numerical schemes.

Although we invested more than twice as much CPU time (in absolute terms) in one dimensional lattices, the results are significantly noisier than for two dimensional lattices. Providing a sufficient number of correction terms still produces consistent data (Table IV), but the results for two dimensional lattices are clearly superior. In fact, the error bar on the exponents for two dimensional lattices is typically half that of one dimensional lattices.

It is known that the Manna Model suffers from significant logarithmic corrections [20]. Manna himself noted a “considerable curvature” in what should have been a straight line in a double logarithmic plot [11]. Similarly, Lübeck and Heger [56] found a surprising splitting of the Manna universality class in one dimension, which might also be due to the presence of significant corrections.

The results for the finite size scaling exponents in Table IV suggest that one-dimensional systems are more difficult to fit, with the alternative fitting functions Eq. (13) and Eq. (12) both clearly performing worse than in two dimensions. One might think that some of the prob-

lems are caused by having much higher accuracy in the estimates in one dimension (and thus requiring more correction term, as bad choices for the fitting function can no longer be hidden in a large statistical error), given that we spent, per lattice, typically about five times more CPU time than in two dimensions. The opposite is the case (probably because correlation times grow like a power law of the linear extent which are very large in one dimension): Depending on the observable, relative errors are between a factor 2 and 10 worse in simple chain compared to square lattice. This holds similarly for other lattices, except for the nnn chain, on which we spent less than 1/6 of the CPU time we spent on the other one dimensional lattices.

In general the relative statistical error vanishes like the inverse square of the CPU time, so that the product of the two gives a measure of “efficiency” of a lattice. Using that measure, the simple chain is the most efficient, followed by nnn chain, rope ladder and finally the Futatsubishi lattice, which is about a factor 4 less efficient (4 times the CPU time is needed for results with similar relative error). This statement, however, is put in perspective, by noting that we used variety of different hardware throughout. The two-dimensional lattices fall roughly in three classes: nc diagonal square lattice, Kagomé lattice, jagged lattice, square lattice, followed by triangular lattice, Archimedes lattice and Mitsubishi lattice, and finally the honeycomb lattice. The latter is clearly the worse (again by about a factor 4), while the triangular lattice is in the first group for some of the observables.

There is a caveat, however. Within a given amount of CPU time and for a given system size, the nc diagonal square lattice (Fig. 2(d)) produces a larger number of avalanches, which are typically much smaller than those for other lattices, because the fraction of virtual neighbours is about 1.5 times higher for the nc diagonal square lattice than for, say, the honeycomb lattice, so that particles are dissipated more frequently. As a result, statistics are comparatively better for nc diagonal square lattice, which, however, may pose higher demands on correction terms with generally larger amplitudes. We could, however, not identify a systematic behaviour in this respect. For example, the moments of jagged lattice are, within error, the same as for *squarelattice*, yet the latter has a much smaller average fraction of dissipative links. In fact, as discussed below, the same leading order amplitudes are found for the avalanche area distribution across all lattices of the same dimension.

The one dimensional lattice perform particularly badly for the moment ratios. Essentially only those for the area size distribution can be fitted well and then produce fairly consistent results (except for the nnn chain). Originally we expected improved scaling behaviour with the introduction of next nearest neighbour interaction, as it prevents degeneracy issues (and, say conserved quantities) as they are sometimes observed on the simple chain [25, 66]. The two dimensional lattices, with the exception of the triangular lattice, generally behave much bet-

TABLE VII: Comparison of the results in the present work to the estimates found in the literature. Many of the works quoted below have studied variants of the Manna Model. The values taken from [52, 53] and [54] in two dimensions are for the Oslo Model. The exponents marked as DP are those for the directed percolation universality class. They are derived via scaling laws [55].

$d$	reference	$D$	$\tau$	$z$	$\alpha$	$D_a$	$\tau_a$	$-\Sigma$
1	this work	2.253(14)	1.112(6)	1.445(10)	1.18(2)	0.998(3)	1.259(11)	0.26(2)
1	[3]	2.2(1)	1.09(3)	1.47(7)				
1	[20]		1.11(2)		1.18(2)			
1	[56]		1.11(2)		1.17(3)			
1	[54]		1.11(5)		1.17(5)			
1	[52]	2.2496(12)						
1	[53]	2.2509(6)						
1	[57] (DP)	2.328673(12)		1.580745(10)		1		
2	this work	2.750(6)	1.273(2)	1.532(8)	1.4896(96)	1.995(3)	1.382(3)	0.761(13)
2	[11]	2.75	1.28(2)	1.55	1.47(10)			
2	[58]	2.73(2)	1.27(1)	1.50(2)	1.50(1)	2.02(2)	1.35(1)	
2	[39]	2.76(1)		1.54(1)		2.03(1)		0.75(4)
2	[20]		1.30(1)		1.55(4)			
2	[56]		1.28(14)		1.50(3)			
2	[54]		1.26(3)		1.48(3)			
2	[59] (DP)	2.979(2)		1.765(3)		2		

ter, when fitting moment ratios. Given the importance of the boundary conditions, it is remarkable how well all universal quantities addressed in the present work are reproduced, even when some two dimensional lattices like the Kagomé lattice (Fig. 3(b)) and the jagged lattice (Fig. 2(b)) have rather complicated boundaries (although the latter is the square lattice in the thermodynamic limit) and many of the lattices have an aspect ratio of unity only asymptotically.

To our surprise, the amplitudes  $A_{a,n}$  in Eq. (15) obtained when fitting the moments of the area distribution seem to be universal themselves. According to Eq. (7)

$$A_{a,n} = a_a b_a^{n+1-\tau_a} \int_0^\infty dy y^{n-\tau_a} \mathcal{G}_a(y), \quad (25)$$

which is universal provided the metric factors  $a_a$  and  $b_a$  are, which is not normally the case. Since  $D_a = d$ , however, the amplitude  $b_a$  of the cutoff  $b_a L^{D_a}$  is dimensionless. It is therefore reasonable to assume that it is universal. There is no reason, however, to assume that the same should hold for  $a_a$  — the argument that  $a_a$  is determined by normalisation does not hold as Eq. (5) applies only asymptotically, *i.e.* the fraction of small event sizes which do not follow simple scaling can, in principle, vary from lattice to lattice. Moreover,  $a_a$  is dimensionful since  $\tau_a \neq 1$ . Nonetheless, it turns out that it does not vary. As a result, to leading order, the moments of the

avalanche areas in one dimension follow

$$\langle a^1 \rangle = [2.01(7)] N^{2-1.259(11)} \quad (26)$$

$$\langle a^2 \rangle = [1.21(5)] N^{3-1.259(11)} \quad (27)$$

$$\langle a^3 \rangle = [0.96(4)] N^{4-1.259(11)} \quad (28)$$

$$\langle a^4 \rangle = [0.83(4)] N^{5-1.259(11)} \quad (29)$$

$$\langle a^5 \rangle = [0.76(4)] N^{6-1.259(11)} \quad (30)$$

and in two dimensions

$$\langle a^1 \rangle = [0.756(7)] N^{2-1.382(3)} \quad (31)$$

$$\langle a^2 \rangle = 0.217(3) N^{3-1.382(3)} \quad (32)$$

$$\langle a^3 \rangle = 0.109(3) N^{4-1.382(3)} \quad (33)$$

$$\langle a^4 \rangle = 0.066(3) N^{5-1.382(3)} \quad (34)$$

$$\langle a^5 \rangle = 0.045(2) N^{6-1.382(3)} \quad (35)$$

as a function of the number  $N$  of sites, independent of the lattice type. We need to qualify the statement, by pointing out that in one dimension the amplitudes across different lattices are rather noisy, and in two dimension the amplitude of  $\langle a^1 \rangle$  has a goodness of fit of just under 0.1 (we are using the  $[\cdot]$  notation again here), while the other results in two dimensions all have a goodness of fit better than 0.5.

Remarkably, had we fitted the area moments against a lattice-dependent multiple of  $N^{1/2}$ , such as the perceived linear extent of the lattice, then this multiplier would have shown in the resulting amplitude  $A_{a,n}$ . and so the apparently universal behaviour would not have come to light.

As explained above, the fitting function is a *hypothesis* and ultimately has an impact on the results. As the number of free parameters increases so does the susceptibility of the result on the initial condition. The approach described above, using fairly large systems (with weaker corrections) with not too small error bars, in conjunction with simple fitting functions, the initial values of which are determined by those with fewer terms, seems to produce robust and reliable results. Comparing the results based on Eq. (15) and Eq. (13) in Table IV to those on the basis of Eq. (12) indicates that the former are superior. An acceptable goodness of fit is reached for Eq. (12) only for those exponents that coincide within a bit more than one standard deviation with the estimates based on Eq. (15). Eq. (13), on the other hand, in summary (Table IV) coincides with Eq. (15), but some, individual finite size scaling exponents, such as  $\mu_1^{(s)}$ , but also  $\Sigma_x$

and  $D_a$ , were estimated too poorly.

In summary, the present work confirms the Abelian Manna Model as an SOC model that displays non-trivial, robust, reproducible, universal scaling behaviour in one and two dimension across different lattices.

### Acknowledgments

H. N. Huynh gratefully acknowledges the hospitality of Department of Mathematics, Imperial College London and GP that of the Department of Physics at NTU Singapore. The authors are indebted to Andy Thomas, Dan Moore and Niall Adams for running the SCAN computing facility at the Department of Mathematics of Imperial College London.

- 
- [1] P. Bak, C. Tang, and K. Wiesenfeld, Phys. Rev. Lett. **59**, 381 (1987).
- [2] K. Christensen and Z. Olami, Phys. Rev. A **46**, 1829 (1992).
- [3] H. Nakanishi and K. Sneppen, Phys. Rev. E **55**, 4012 (1997).
- [4] A. Ben-Hur and O. Biham, Phys. Rev. E **53**, R1317 (1996).
- [5] D. Dhar, Physica A **369**, 29 (2006), proceedings of the *11th International Summerschool on "Fundamental Problems in Statistical Physics"*, Leuven, Belgium, Sep 4 – 17, 2005.
- [6] J. A. M. S. Duarte (1990), cited in [67] as private communication for studying the BTW model on a triangular lattice.
- [7] S. S. Manna, Physica A **179**, 249 (1991).
- [8] C.-K. Hu and C.-Y. Lin, Physica A **318**, 92 (2003), ISSN 0378-4371.
- [9] N. Azimi-Tafreshi, H. Dashti-Naserabadi, S. Moghimi-Araghi, and P. Ruelle, J. Stat. Mech. **2010**, P02004 (2010), arXiv:0912.3331v2.
- [10] H. N. Huynh, L. Y. Chew, and G. Pruessner, Phys. Rev. E **82**, 042103 (pages 4) (2010), arXiv:1006.5807.
- [11] S. S. Manna, J. Phys. A: Math. Gen. **24**, L363 (1991).
- [12] I. Syözi, Prog. Theor. Phys. **6**, 306 (1951).
- [13] C. Itzykson and J.-M. Drouffe, *Statistical field theory*, vol. 1 (Cambridge University Press, Cambridge, UK, 1997), 1st ed.
- [14] D. Dhar, Physica A **263**, 4 (1999), proceedings of the *20th IUPAP International Conference on Statistical Physics*, Paris, France, Jul 20–24, 1998, arXiv:cond-mat/9808047.
- [15] K. Christensen, Á. Corral, V. Frette, J. Feder, and T. Jøssang, Phys. Rev. Lett. **77**, 107 (1996).
- [16] G. Pruessner and H. J. Jensen, Phys. Rev. E **65**, 056707 (pages 8) (2002), arXiv:cond-mat/0201306.
- [17] P. Grassberger, New J. Phys. **4**, 17 (pages 15) (2002), arXiv:cond-mat/0202022.
- [18] P. L. Dorn, D. S. Hughes, and K. Christensen (2001), preprint from [http://www.cmth.ph.ic.ac.uk/kim/papers/preprints/preprint\\_btw.pdf](http://www.cmth.ph.ic.ac.uk/kim/papers/preprints/preprint_btw.pdf), accessed 19 Oct 2010.
- [19] Z. Olami, H. J. S. Feder, and K. Christensen, Phys. Rev. Lett. **68**, 1244 (1992).
- [20] R. Dickman and J. M. M. Campelo, Phys. Rev. E **67**, 066111 (pages 5) (2003).
- [21] D. Dhar (1999), overlaps with [14], updated in [5]., arXiv:cond-mat/9909009.
- [22] T. M. Liggett, *Stochastic Interacting Systems: Contact, Voter and Exclusion Processes* (Springer-Verlag, Berlin, Germany, 2005).
- [23] P. C. Hohenberg and B. I. Halperin, Rev. Mod. Phys. **49**, 435 (1977).
- [24] M. Paczuski and K. E. Bassler (2000), according to [25], this is probably the correct version of [68]., arXiv:cond-mat/0005340v2.
- [25] D. Hughes and M. Paczuski, Phys. Rev. Lett. **88**, 054302 (pages 4) (2002).
- [26] B. Grünbaum and G. C. Shephard, *Tilings and patterns* (Freeman and Company, New York, NY, USA, 1987).
- [27] I. Syözi, in *Phase Transitions and Critical Phenomena*, edited by C. Domb and M. S. Green (Academic Press, London, UK, 1972), vol. 2, pp. 269–329.
- [28] R. J. Baxter, *Exactly Solved Models in Statistical Mechanics* (Dover Publications, Inc., New York, NY, USA, 2007).
- [29] M. Loeb, *Discrete Mathematics in Statistical Physics* (Vieweg+Teubner, Wiesbaden, Germany, 2010).
- [30] M. Paczuski and S. Boettcher, Phys. Rev. Lett. **77**, 111 (1996).
- [31] G. Pruessner, J. Phys. A: Math. Gen. **37**, 7455 (2004), arXiv:cond-mat/0402564.
- [32] J. Morand, G. Pruessner, and K. Christensen (2010), to be published.
- [33] B. Efron, *The Jackknife, the Bootstrap and Other Resampling Plans* (SIAM, Philadelphia, PA, USA, 1982).
- [34] M. Matsumoto and T. Nishimura, ACM Trans. Model. Comp. Sim. **8**, 3 (1998).
- [35] G. Marsaglia, *Mersenne twister*, newsgroup posting 14 Jul 2005, 12:04am, accessed 10 May 2011, URL [http://groups.google.com/group/sci.crypt/browse\\_thread/thread/305c507efbe85be4](http://groups.google.com/group/sci.crypt/browse_thread/thread/305c507efbe85be4).

- [36] G. Marsaglia, *Random numbers for c: The end?*, newsgroup posting 20 Jan 1999, 9:00am, accessed 10 May 2011, URL <https://groups.google.com/group/sci.math.num-analysis/msg/eb4ddde782b17051>.
- [37] S. Brandt, *Data Analysis* (Springer-Verlag, Berlin, Germany, 1998).
- [38] G. Pruessner and N. R. Moloney, *J. Phys. A: Math. Gen.* **36**, 11213 (2003), arXiv:cond-mat/0309126.
- [39] S. Lübeck, *Phys. Rev. E* **61**, 204 (2000).
- [40] M. De Menech, A. L. Stella, and C. Tebaldi, *Phys. Rev. E* **58**, R2677 (1998).
- [41] K. Christensen, N. Farid, G. Pruessner, and M. Stapleton, *Eur. Phys. J. B* **62**, 331 (2008).
- [42] A. Chessa, H. E. Stanley, A. Vespignani, and S. Zapperi, *Phys. Rev. E* **59**, R12 (1999).
- [43] G. Pruessner and H. J. Jensen, *Phys. Rev. E* **70**, 066707 (pages 25) (2004), arXiv:cond-mat/0309173.
- [44] H. J. Jensen, K. Christensen, and H. C. Fogedby, *Phys. Rev. B* **40**, 7425 (1989).
- [45] K. Christensen, H. C. Fogedby, and H. J. Jensen, *J. Stat. Phys.* **63**, 653 (1991).
- [46] K. Christensen and Z. Olami, *Phys. Rev. E* **48**, 3361 (1993).
- [47] F. J. Wegner, *Phys. Rev. B* **5**, 4529 (1972).
- [48] W. H. Press, S. A. Teukolsky, W. T. Vetterling, and B. P. Flannery, *Numerical Recipes in C* (Cambridge University Press, New York, NY, USA, 1992), 2nd ed.
- [49] K. Binder, *Z. Phys. B* **43**, 119 (1981).
- [50] K. Binder, *Phys. Rev. Lett.* **47**, 693 (1981).
- [51] V. Privman, P. C. Hohenberg, and A. Aharony, in *Phase Transitions and Critical Phenomena*, edited by C. Domb and J. L. Lebowitz (Academic Press, New York, NY, USA, 1991), vol. 14, chap. 1, pp. 1–134.
- [52] K. Christensen, *Physica A* **340**, 527 (2004), proceedings of the symposium *Complexity and Criticality: in memory of Per Bak (1947–2002)*, Copenhagen, Denmark, Aug 21–23, 2003.
- [53] G. Pruessner, Ph.D. thesis, Imperial College London, 180 Queen’s Gate, London SW7 2BZ, UK (2004), accessed 19 Nov 2009, URL [http://www.ma.imperial.ac.uk/~pruess/publications/thesis\\_final/](http://www.ma.imperial.ac.uk/~pruess/publications/thesis_final/).
- [54] J. A. Bonachela, Ph.D. thesis, Departamento de Electromagnetismo y Física de la Materia & Institute Carlos I for Theoretical and Computational Physics, University of Granada, Granada, Spain (2008), accessed 12 Sep 2009, URL <http://hera.ugr.es/tesisugr/17706312.pdf>.
- [55] S. Lübeck, *Int. J. Mod. Phys. B* **18**, 3977 (2004).
- [56] S. Lübeck and P. C. Heger, *Phys. Rev. E* **68**, 056102 (pages 11) (2003).
- [57] I. Jensen, *J. Phys. A: Math. Gen.* **32**, 5233 (1999).
- [58] A. Chessa, A. Vespignani, and S. Zapperi, *Comp. Phys. Comm.* **121–122**, 299 (1999), proceedings of the *Europhysics Conference on Computational Physics CCP 1998*, Granada, Spain, Sep 2–5, 1998.
- [59] C. A. Voigt and R. M. Ziff, *Phys. Rev. E* **56**, R6241 (1997).
- [60] A. Vespignani, R. Dickman, M. A. Muñoz, and S. Zapperi, *Phys. Rev. E* **62**, 4564 (2000), arXiv:cond-mat/0003285.
- [61] J. A. Bonachela and M. A. Muñoz, *Physica A* **384**, 89 (2007), ISSN 0378-4371, proceedings of the *International Conference on Statistical Physics*, Raichak and Kolkata, India, Jan 5–9, 2007.
- [62] J. A. Bonachela and M. A. Muñoz, *Phys. Rev. E* **78**, 041102 (pages 8) (2008), arXiv:0806.4079.
- [63] J. Marro and R. Dickman, *Nonequilibrium Phase Transitions in Lattice Models* (Cambridge University Press, New York, NY, USA, 1999).
- [64] G. Pruessner, *Phys. Rev. E* **76**, 061103 (pages 4) (2007), arXiv:0712.0979v1.
- [65] G. Pruessner, *New J. Phys.* **10**, 113003 (pages 13) (2008), arXiv:0706.1144.
- [66] D. Dhar and R. Ramaswamy, *Phys. Rev. Lett.* **63**, 1659 (1989).
- [67] S. S. Manna, *J. Stat. Phys.* **59**, 509 (1990).
- [68] M. Paczuski and K. E. Bassler, *Phys. Rev. E* **62**, 5347 (2000), according to [25], this(?) version “was published by mistake. The correct version is [...] arXiv:cond-mat/0005340”. This probably means arXiv:cond-mat/0005340v2.
- [69] In hindsight, the lattices used in two dimensions appear rather small compared to one, as the CPU time required is essentially determined by the linear extent,  $N^{1/2}$ .
- [70] Voigt and Ziff follow a different notation;  $2/z$  in their work [59] corresponds to  $z$  here and their  $2\eta/z$  to  $\beta/\nu_{\perp}$  here.